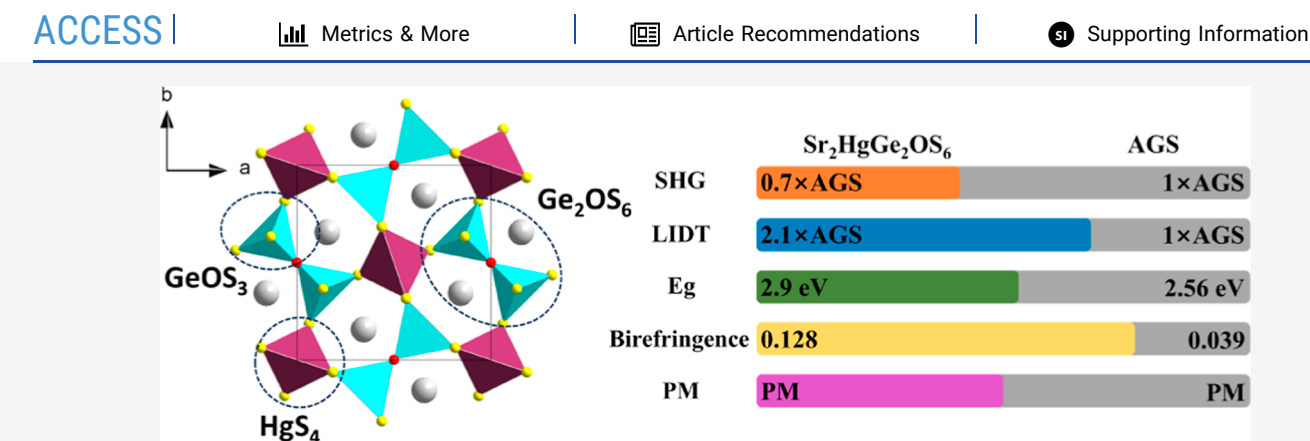
Inorganic Chemistry

pubs.acs.org/IC Article

Sr₂HgGe₂OS₆: A Hg-Based Oxychalcogenide Infrared Nonlinear Optical Material Exhibiting Favorable Balance between a Large Band Gap and Strong Second Harmonic Generation Response

Guili Wang, Chunxiao Li, Ming-Hsien Lee,* and Jiyong Yao*





ABSTRACT: Currently, oxychalcogenides with mixed-anion groups that integrate the property advantages of oxides (wide optical band gap) and chalcogenides [strong second harmonic generation (SHG) response] through chemical substitution engineering have attracted widespread interest and are considered to be important candidates for infrared (IR) nonlinear optical (NLO) materials. Herein, the first Hg-based oxychalcogenide $Sr_2HgGe_2OS_6$ with mixed anion [GeOS₃] units has been successfully synthesized through a spontaneous crystallization method, which exhibits a favorable balance between the strong SHG response $(0.7 \times AgGaS_2)$ and large optical band gap (2.9 eV). In addition, $Sr_2HgGe_2OS_6$ shows high laser-induced damage threshold (LIDT, $2.1 \times AgGaS_2$) as well as phase-matching (PM) performance. Theoretical calculations indicate that the $Sr_2HgGe_2OS_6$ encompasses large birefringence of 0.128@2090 nm $(3.3 \times AgGaS_2)$ and its SHG density mainly comes from $[HgS_4]$ tetrahedra and $[GeOS_3]$ units. This work not only demonstrates that $Sr_2HgGe_2OS_6$ is a promising IR NLO material but also provides new ideas for the exploration of Hg-based oxychalcogenide IR NLO materials.

INTRODUCTION

Nonlinear optical (NLO) materials are the key component of all-solid-state laser frequency conversion system that can generate nonlinear polarization under laser irradiation and convert the known wavelength lasers into ultraviolet (UV), visible, and infrared (IR) wavelength lasers through the frequency conversion technology like second harmonic generation (SHG),¹ optical parametric amplification,² and optical parametric oscillation,³ which effectively broaden the wavelength range of the laser output.

IR NLO crystals can convert mature near-IR or visible lasers to realize the laser output in the mid/far-IR bands, and the coherent light source in this band has very important application value in numerous fields, such as communication, medicine, environmental monitoring, civil industries, etc.^{4–8} Although the commercially available IR NLO crystals, such as ZnGeP₂ (ZGP), AgGaS₂ (AGS), and AgGaSe₂ (AGSe)¹¹ have large SHG coefficients and wide IR transmission ranges, these crystals have intrinsic defects, including strong

absorption of 1–2 μ m pumping laser light for ZGP, low laser-induced damage thresholds (LIDTs) for AGS and AGSe, and multiphonon absorption of AGS and ZGP near 9 μ m, which limit their wider applications. ^{9,12–14} Although many other types of IR NLO crystals have been discovered by researchers over the years, their comprehensive performances are not outstanding enough. Therefore, exploring new reliable mid- and far-IR NLO crystals is still very necessary. ^{15–17}

From the point of view of practical application, fulfilling the following four performance requirements is highly advantageous for new IR NLO crystals: (i) strong SHG response (\geq 1 × AGS); (ii) wide optical band gap ($E_g > 2.33$ eV) along with

Received: March 7, 2024 Revised: May 8, 2024 Accepted: May 13, 2024 Published: May 23, 2024





high LIDT; (iii) wide IR transmission range (particularly for the two "3-5" and "8-12 μ m" atmospheric transparent windows); and (iv) appropriate birefringence ($\Delta n > 0.04$) for phase-matching (PM) behavior. At the same time, the crystals should also be stable in the air as well as easy to grow and process. However, it is a great challenge to achieve a positive balance of the above parameters. Notably, in recent studies, oxychalcogenides with mixed anionic moieties have attracted wide interest and are considered to be an important class of IR NLO candidates due to their ability to combine the strengths of oxides (wide band gap) and chalcogenides (large SHG response) effectively. Driven by the above strategy, a substantial amount of NLO materials have been synthesized and characterized, such as $La_3Ga_3Ge_2O_{10}S_3$, 18 $Sr_5Ga_8O_3S_{14}$, 19 $Ae_3Q[GeOQ_3]$ (Ae = Ba, Sr; Q = S, Se), 20 AeGeS₂O (Ae = Ba, Sr, Qae = S, Se), 20 AeGeS₂O (Ae = Sa, Se), 20 AeGeS₂O (A Sr), 21 A₂MM₂′OS₆ (A = Ca, Sr, Eu; M = Zn, Cd, Mn, Fe, Co, Ge; M′ = Ge, Sn, Ga), $^{22-29}$ Sr₃Ge₂O₄Se₃, 30 Ae₃Ge₂O₄Te₃ (Ae = Ba, Sr), 31,32 etc. $^{33-35}$ Most of them have demonstrated surprising performance. However, Hg-based oxychalcogenide IR NLO materials have never been reported, as far as we know. Actually, Hg-based IR NLO materials are attractive for the following reasons: (i) Hg²⁺ cation possesses highly polarizable and deformable electron clouds, which can enhance the NLO intensity and birefringence to a certain extent; (ii) Hg is conducive to the enlargement of the IR transparent range as a heavy metal element; (iii) Hg atom has multiple coordination modes with chalcogen in linear, triangular, and tetrahedral modes, which not only increases the structural diversity but also enables the opportunity to obtain strong NLO effects.^{36–40}

After much effort, the first Hg-based oxychalcogenide IR NLO material $Sr_2HgGe_2OS_6$ with highly polarized $[GeOS_3]$ units was successfully synthesized via the spontaneous crystallization method. It crystallizes in the noncentrosymmetric (NCS) tetragonal space group $P\overline{4}2_1m$ (no. 113). Experimental results indicate a strong SHG response (0.7 × AGS), wide optical bandgap (2.9 eV) along with high LIDT (2.1 × AGS), and PM behavior. In addition, theoretical calculations display that the $Sr_2HgGe_2OS_6$ encompasses a large birefringence of 0.128@2090 nm (3.3 × AGS) and its strong SHG response mainly comes from the highly polarized $[GeOS_3]$ units and $[HgS_4]$ tetrahedra.

EXPERIMENTAL SECTION

Reagents. Caution! Toxic HgS was used; safeguards should be taken. All highly purified raw materials, Sr (99.99%), HgS (99.99%), S (99.999%), Ge (99.999%), GeO₂ (99.999%), and CsI (99.9%), were commercially purchased from the Aladdin Co., Ltd. without further purification and stored in an Ar-filled glovebox. By heating the stoichiometric mixture of raw elements in flame-sealed silica tubes under a vacuum of 10^{-3} Pa, the binary compounds SrS and GeS₂ were synthesized.

Single-Crystal Growth. The spontaneous crystallization method was used to obtain $Sr_2HgGe_2OS_6$ single crystals. First, the mixture of raw materials (molar ratio $SrS/HgS/GeO_2/GeS_2=2:1:0.5:1.5$, total mass 0.3 g) was thoroughly ground together with CsI (0.3 g) as flux and loaded into a quartz tube. The tube was then evacuated to 10^{-3} Pa, sealed by using a hydroxide flamer, and placed into a programmed muffle furnace. The furnace was slowly heated to 1123 K within 30 h and maintained for 24 h to homogenize the reactant, then cooled to 673 K gradually at a rate of 3 K/h. Finally, the furnace was turned off and the temperature was cooled to room temperature (RT). The yellow transparent crystals of $Sr_2HgGe_2OS_6$ were obtained, and they are insensitive to oxygen and moisture in the air.

Structure Determination. The single-crystal X-ray diffraction measurement of a suitable $Sr_2HgGe_2OS_6$ crystal was carried out at 296.15 K employing a Bruker D8 Quest diffractometer with a Mo- K_{α} (λ = 0.71073 Å) radiation source equipped with a CCD area detector. The structure of $Sr_2HgGe_2OS_6$ was solved with the olex2.solve structure solution program⁴¹ using charge flipping and refined with the SHELXL-2018 refinement package⁴² using least squares minimization. Absorption correction was made by the multi-scan method. The crystallographic data and structure refinement details of $Sr_2HgGe_2OS_6$ are exhibited in Table 1.

Table 1. Crystallographic Data and Structure Refinement for Sr₂HgGe₂OS₆^a

empirical formula	$Sr_2HgGe_2OS_6$
formula weight	729.37
crystal system	tetragonal
space group	$P\overline{4}2_1m$
a (Å)	9.6240(4)
b (Å)	9.6240(4)
c (Å)	6.1904(4)
α (°), β (°), and γ (°)	90
volume (ų)	573.36(6)
Z	2
$ ho_{\rm calc}~({ m g/cm^3})$	4.225
$\mu \left(\mathrm{mm}^{-1}\right)$	28.807
F(000)	648.0
radiation	Mo K_{α} ($\lambda = 0.71073$)
2 heta range for data collection (°)	5.986-60.956
index ranges	$-11 \le h \le 13, -13 \le k \le 12, -8 \le l \le 8$
independent reflections	944 [$R_{\text{int}} = 0.0736$, $R_{\text{sigma}} = 0.0569$]
data/restraints/parameters	944/0/36
goodness-of-fit on F ²	1.054
final R indexes $[I \ge 2\sigma(I)]$	$R_1 = 0.0323$, $wR_2 = 0.0569$
final R indexes [all data]	$R_1 = 0.0436$, $wR_2 = 0.0615$
flack parameter	0.03(2)
$^{a}R_{1} = \Sigma F_{0} - F_{c} /\Sigma F_{0} , wR_{2} = [\Sigma w(F_{0}^{2} - F_{c}^{2})^{2}/\Sigma wF_{0}^{4}]^{1/2} \text{ for } F_{0}^{2} > 0$	
$2\sigma(F_0^2)$.	

Elemental Analysis. Elemental analysis was performed on a $Sr_2HgGe_2OS_6$ single crystal using a HITACHI S-4300 scanning electron microscope (accelerating voltage 15 kV) equipped with an OXFORD X-Max^N 80 energy-dispersive X-ray spectroscope (EDS).

Polycrystalline Synthesis. Considering the decomposition property of HgS at high temperatures, the polycrystalline of $Sr_2HgGe_2OS_6$ was synthesized by solid-state reaction at the nonstoichiometric ratio. The mixture of raw materials (molar ratio $SrS/HgS/GeO_2/Ge/S = 2:1.4:0.5:1.5:2.6$) was ground finely using an agate mortar and placed into a quartz tube inside the glovebox. Before heating, the tube was evacuated to 1×10^{-3} Pa and flame sealed. In the first step, the mixture was gradually heated to 873 K in 24 h and kept for 72 h, finally cooled to RT slowly. In the second step, the presintered sample was reheated to 1023 K and held for 72 h, followed by a slow cooling to RT. The Hg pure element produced by decomposition in the sample was then removed and the sample was reground for subsequent tests.

Powder X-ray Diffraction (PXRD). A Bruker D8 advance diffractometer equipped with Cu-K_{α} ($\lambda=1.5418~\text{Å}$) radiation was employed to obtain PXRD pattern of $\text{Sr}_2\text{HgGe}_2\text{OS}_6$ from 10 to 70° within a scanning step width of 0.02° at 40 kV, 40 mA, and RT. The simulated pattern is generated by Mercury software.

IR Spectroscopy. The polycrystalline $Sr_2HgGe_2OS_6$ was mixed with dry KBr and ground thoroughly at a mass ratio of 1:100, and its IR spectral data was collected by an Excalibur 3100 Fourier transform IR spectrometer from 400 to 4000 cm $^{-1}$.

UV-Vis-NIR Diffuse Reflectance Spectroscopy. An Agilent Carry 7000 UV-vis-NIR spectrophotometer equipped with an

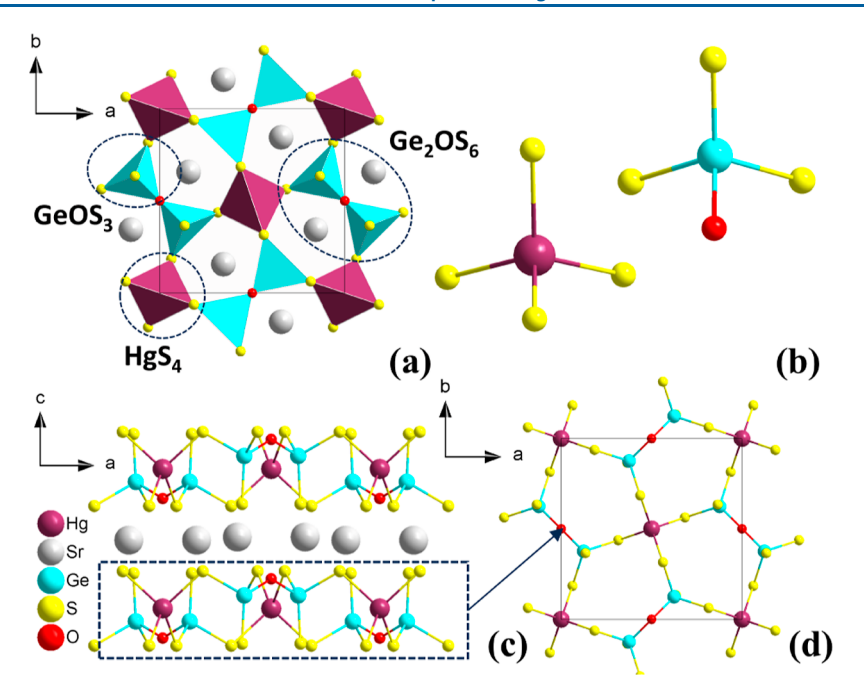


Figure 1. Schematic illustration of the crystal structure for $Sr_2HgGe_2OS_6$ (hiding Sr-O and Sr-S bonds for a better view): (a) view from the c axis; (b) $[HgS_4]$ tetrahedron and $[GeOS_3]$ unit; (c) view from the b axis; and (d) 2D $[HgGe_2OS_6]_{\infty}$ layers view along the ab-plane.

integrating sphere was used to measure the UV–vis–NIR diffuse reflectance spectrum of $\rm Sr_2HgGe_2OS_6$ polycrystalline in the wavelength range of 200–2500 nm. A polytetrafluoroethylene standard sample with 100% reflectance was used as a reference. The absorption data was calculated from the reflectance data through the Kubelka–Munk function. 43

Powder SHG Measurement. The size-dependent SHG intensity of $\rm Sr_2HgGe_2OS_6$ polycrystalline was estimated through the Kurtz–Perry technique⁴⁴ using a 2090 nm Q-switch Ho:Tm:Cr:YAG fundamental laser. The polycrystalline of $\rm Sr_2HgGe_2OS_6$ was sieved into six different particle size ranges (20–50, 50–90, 90–125, 125–150, 150–200, and 200–224 μ m) and loaded into customized holders with a thickness of 0.5 mm. Likewise, the microcrystals of AGS were sieved into the same particle ranges as standard samples.

Powder LIDT Measurement. The powder LIDT of $Sr_2HgGe_2OS_6$ sample (200–224 μ m) was measured by single-pulse method⁴⁵ using a 1064 nm pulsed Nd:YAG laser with the same particle size AGS powder as a reference. The samples were fixed in custom-made aluminum holders with the use of glass coverslips and rubber pads with a thickness of 0.5 mm, then placed in the experimental light path, and irradiated by the pulsed laser (pulse width $\tau_p=5$ ns; repetition frequency = 1 Hz). The laser power was increased continuously, and the samples were observed under an optical microscope until the samples showed a bright spot due to damage, at which time the laser beam power (E) and damage spot area (E) were recorded. Subsequently, the LIDTs of E0 signal and AGS samples were calculated according to the following equation: LIDT = E10 signal and E10 signal according to the following equation: LIDT = E10 signal according to the following equation:

Computational Details. To better understand the structure–property relationship of Sr₂HgGe₂OS₆, CASTEP, ⁴⁶ a density-functional theory-based planewave pseudopotential code, was used to perform the first-principles calculations. The exchange–correlation potential in the calculation of Sr₂HgGe₂OS₆ was described using the Perdew–Burke–Ernzerhof (PBE) functional within the generalized gradient approximation (GGA).⁴⁷ Soft norm-conserving pseudopotentials ⁴⁸ was used in the present study, Ge treats 4 instead of 14 electrons as valence, $E_{\rm cut}$ 600 eV was used in all the calculations. k-point sampling of 0.04 Å⁻¹ was used for both self-consistent field (SCF) and non-SCF (optical properties) calculations; such sampling is sufficient to converge birefringence and SHG coefficients. As for optical properties, the scissor operation was applied to match the

experimental value by the shift of conduction band (CB). Additionally, SHG susceptibilities d_{ij} and SHG density of virtual electronic occupied (VE occ) and virtual hole unoccupied (VH unocc) states were calculated on the basis of a sum-over-state type formalism called optical and visualization program, separately. According to the Kramers-Kronics transform, the refractive index was also calculated.

■ RESULTS AND DISCUSSION

Crystal Structure and Elemental Analysis. The singlecrystal X-ray diffraction demonstrates that the melilite-type oxychalcogenide Sr₂HgGe₂OS₆ crystallizes in the NCS tetragonal space group $P\overline{4}2_1m$ (no. 113) with unit cell parameters of a = b = 9.6240(4) Å, c = 6.1904(4) Å, and Z = 2. In its independent asymmetric unit, there are one Sr, one Hg, one Ge, one O, and two S atoms (Table S1). The valences of the elements Sr, Hg, Ge, O, S1, and S2 were determined to be 1.950, 2.394, 4.033, -1.840, -2.223, and -1.814, respectively, based on the calculated bond valence sums (BVS), as displayed in Table S1, which are consistent with the structural analysis. This also indicates that the structure of Sr₂HgGe₂OS₆ is reasonable. The coordination environments and bond lengths for Sr, Hg, and Ge cation sites of Sr₂HgGe₂OS₆ are shown in Figure S1. Each Ge atom is fourcoordinated with two S1 atoms, one S2 atom, and one O atom to form a mixed-anion [GeOS₃] unit with a Ge-O bond length of 1.845(5) Å (Figures 1b and S1a), which is reasonable compared with the 1.834 Å discovered in Sr₂CdGe₂OS₆.²⁷ The Ge-S bond lengths of 2.140(4)-2.211(1) Å are equivalent to the 2.205(3)-2.210(4) Å range reported in $Sr_3S[GeOS_3]^{20}$ Each Hg atom is coordinated with four S1 atoms to form the typical [HgS₄] tetrahedron with four identical Hg-S bond lengths of 2.498(2) Å (Figures 1b and S1b), which is also comparable to the result of 2.405(4)-2.920(3) Å reported in KHg₄Ga₃S₉. In the structure of Sr₂HgGe₂OS₆, two neighboring [GeOS₃] units form [Ge₂OS₆] dimers by sharing O atoms, then the [Ge₂OS₆] dimers are connected to the $[HgS_4]$ tetrahedra by sharing S1 atoms, as shown in Figure 1a. These units further form two-dimensional (2D) [HgGe₂OS₆]_m

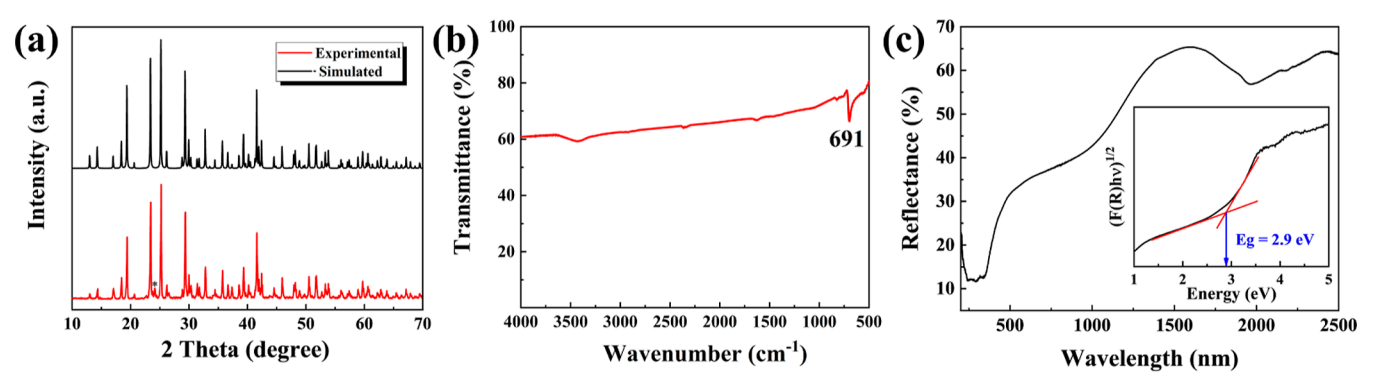


Figure 2. (a) Simulated and experimental powder X-ray diffraction patterns (* indicates S_8 impurity); (b) IR spectrum; and (c) UV-vis-NIR diffuse reflectance spectrum of $Sr_2HgGe_2OS_6$.

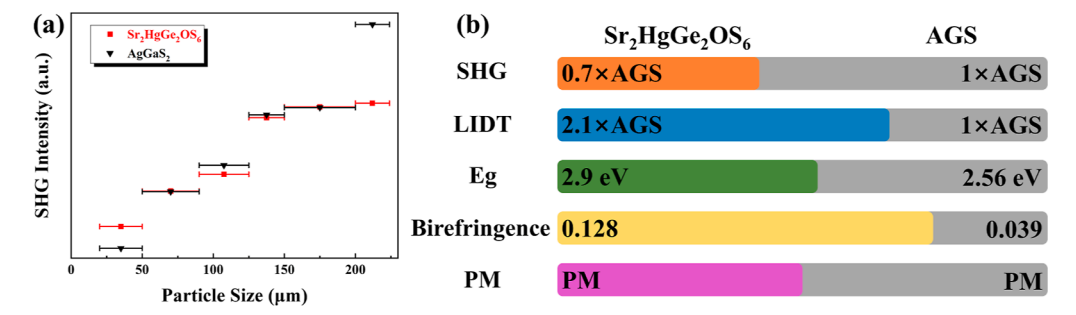


Figure 3. (a) SHG intensity versus particle size, and (b) NLO performance comparison of Sr₂HgGe₂OS₆ and AgGaS₂.

PXRD. Based on the comparison diagram in Figure 2a, it is evident that the main phase of the experimental pattern is in good agreement with the simulated pattern, but there are trace amounts of centrosymmetric S_8 impurity, which could not be removed after many attempts; we speculate that this is due to the high-temperature decomposition characteristic of HgS. Considering its low content and centrosymmetric structure, the impact on the results of subsequent tests can be ignored.

Optical Properties. The IR and UV–vis–NIR diffuse reflectance spectra of $Sr_2HgGe_2OS_6$ are illustrated in Figure 2b,c. It is clear that $Sr_2HgGe_2OS_6$ has a relatively high transmittance in the range of $4000-700~cm^{-1}$, corresponding to $2.5-14.2~\mu m$, covering the atmospheric transparent windows of "3–5" and "8–12 μm ". The only distinct absorption peak at 691 cm⁻¹ in the IR spectrum is attributed to Ge–O stretching mode.²⁹ The broad band at about 3300 cm⁻¹ in the IR spectrum due to the symmetric O–H stretching mode of H_2O adsorbed in the sample.^{50,51} In addition, the experimental band gap of $Sr_2HgGe_2OS_6$ is concluded to be 2.9 eV (the inserted spectrum in Figure 2c) according to the

Kubelka–Munk function, 43 which is consistent with the yellow color of $Sr_2HgGe_2OS_6$ crystal. Obviously, the band gap of $Sr_2HgGe_2OS_6$ is larger than those of traditional IR NLO materials AGS (2.56 eV), 52 AGSe (1.73 eV), 53 and ZGP (2.02 eV), 54 implying that the $Sr_2HgGe_2OS_6$ may possess high LIDT than these commercial materials.

Powder LIDT and SHG Properties. LIDT value is a very important parameter for IR NLO materials. Thus, the powder LIDT of Sr₂HgGe₂OS₆ was also tested to evaluate its NLO performance using a 1064 nm pulsed Nd:YAG laser with the AGS powder as a reference. Starting from 0.1 mJ, the energy of the incident laser was progressively increased until the damage point is visible under an optical microscope. 0.47 and 0.22 mJ were recorded as the cutoff energies of Sr₂HgGe₂OS₆ and AGS, respectively. As shown in Table S5, the experimental LIDT result of Sr₂HgGe₂OS₆ is about 74.80 MW cm⁻², 2.1 times as much as that of AGS (35.01 MW cm⁻²), hinting at the possibility of Sr₂HgGe₂OS₆'s application in a higher power laser than AGS. However, this powder LIDT value is not large enough. In order to improve the LIDT of Sr₂HgGe₂OS₆ for high-power laser applications, measures such as growing highquality crystals, selecting coating materials with high damage thresholds, and suitable coating methods can be taken. $Sr_2HgGe_2OS_6$ crystallizes in the NCS space group $P\overline{42}_1m$ (no. 113) and thus, we measured its powder SHG response using a 2.09 µm fundamental laser (Q-switched Ho:Tm:-Cr:YAG) through the Kurtz-Perry method. The reference is AGS with the same particle size. The SHG intensity clearly tends to increase with the increasing particle size and then approaches saturation, which suggests that Sr₂HgGe₂OS₆ can achieve type-I PM and has a strong SHG response approximately 0.7 times that of AGS (Figure 3a). Furthermore, we also compared the NLO properties of title compound and materials for series $A_2MM_2'OS_6$ (A = Ca, Sr, Eu; M = Zn, Cd,

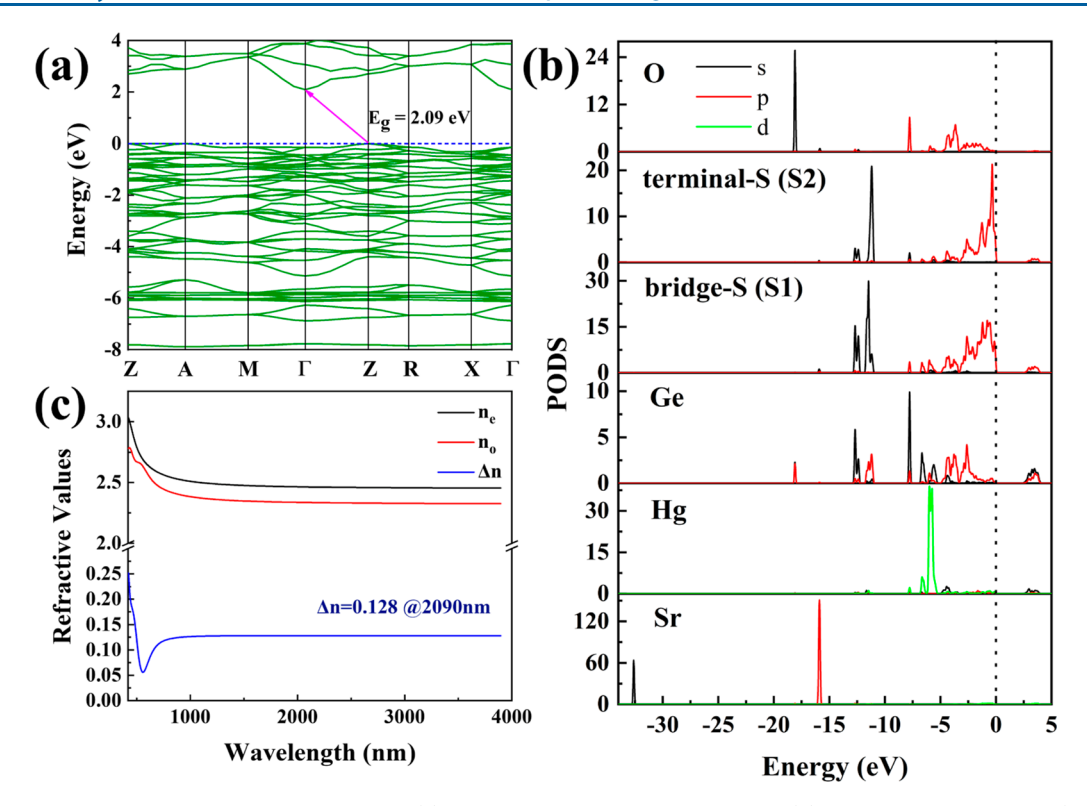


Figure 4. Theoretical calculation results of $Sr_2HgGe_2OS_6$: (a) calculated electronic band structure; (b) partial densities of states (PDOS); and (c) calculated refractive dispersion curve.

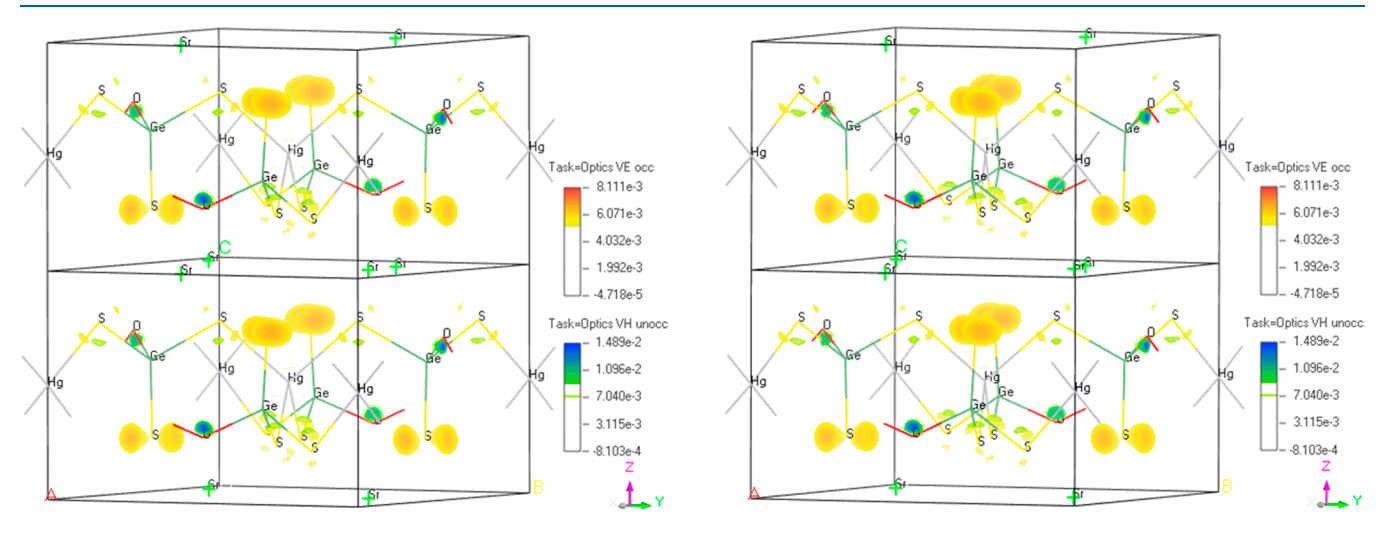


Figure 5. Stereo pair cross-eyed view of SHG-densities of occupied states in the virtual electronic (VE occ) process and unoccupied states in the virtual hole (VH unocc) process of Sr₂HgGe₂OS₆.

Mn, Fe, Co, Ge; M' = Ge, Sn, Ga; Table S4), showing that Sr₂HgGe₂OS₆ achieves a good balance between the strong SHG effect and wide band gap in the same type of melilite materials. All the above experimental results imply that Sr₂HgGe₂OS₆ is a very promising IR NLO material with excellent performances, including strong SHG response, wide optical band gap, and high LIDT along with PM properties (Figure 3b). In particular, from Sr₂ZnGe₂OS₆, Sr₂CdGe₂OS₆ to Sr₂HgGe₂OS₆, it is obvious that the SHG response gradually increase. Although the band gap of Sr₂HgGe₂OS₆ is smaller than theirs, it is also larger than that of the commercial IR NLO material AGS. Therefore, we can speculate that introducing Hg atoms into oxychalcogenide materials can

both improve the SHG response and maintain a relatively large band gap value. This discovery is very attractive and can also be applied to many reported oxychalcogenide systems, further expanding the exploration direction of new IR NLO materials.

Theoretical Calculations. The band structure of Sr₂HgGe₂OS₆ is shown in Figure 4a, indicating that it has an indirect band gap of 2.09 eV, which is smaller than the experimental band gap of 2.9 eV. Considering the provided GGA-PBE exchange−correlation functional, this result is not unexpected. Meanwhile, the PDOS of each element for Sr₂HgGe₂OS₆ were also plotted, as illustrated in Figure 4b. The range from −5 to 0 eV in PDOS is mainly predominated by Ge 4p and S 3p, intermixed with a minor contribution from

O 2p orbitals, while the Ge 4s 4p, Hg 6s, and S 3p orbitals make a major contribution from 2.1 to 5 eV. Due to the decisive role of the tracks on both sides of the band gap in the optical properties of materials, the optical properties of $Sr_2HgGe_2OS_6$ can be inferred to be primarily determined by the $[HgS_4]$ tetrahedra and $[GeOS_3]$ units. Next, also calculated was the birefringence of $Sr_2HgGe_2OS_6$ based on the electronic structure, as shown in Figure 4c, the calculated birefringence value of $Sr_2HgGe_2OS_6$ at 2090 nm is 0.128 without scissor shift or 0.117 with scissor shift of 0.809 eV, which is approximately 3.3 times than that of AGS (0.039@2090 nm). Especially, such a large birefringence value allows $Sr_2HgGe_2OS_6$ to achieve PM behavior, which is in good agreement with the powder SHG experimental results (Figure 3a).

In addition, because Sr₂HgGe₂OS₆ belongs to the NCS space group $P\overline{42}_1m$, there is only one independent SHG coefficient d_{14} within the restriction of Kleinman's symmetry. With and without a scissor shift of 0.809 eV, the SHG coefficients (d₁₄) evaluated for Sr₂HgGe₂OS₆ are 4.526 and 8.505 pm/V, respectively, which are slightly smaller than that of experimental results (Figure 3a). Subsequently, in order to analyze the origin of NLO effect for Sr₂HgGe₂OS₆, SHG density calculations were also performed, as demonstrated in Figure 5, from the cross-eyed stereopair of the occupied states in the virtual electronic (VE occ) process and unoccupied states in the virtual hole (VH unocc) process, there is no SHG density distribution on Sr²⁺ cations, the contribution of VE occupied state mainly comes from terminal-S (S2) atoms, with a small portion coming from Hg and bridge-S (S1) atoms, while the VH unoccupied state of SHG density is composed of O and bridge-S (S1) atoms. In general, the SHG response of Sr₂HgGe₂OS₆ mainly originates from [HgS₄] tetrahedra and mixed-anion [GeOS₃] units. Moreover, the dipole moment (DM) analysis of [GeOS₃] unit and [HgS₄] tetrahedron in Sr₂HgGe₂OS₆ was also carried out employing the bond valence method.⁵⁷ Obviously, the DM of the [GeOS₃] unit is clearly larger than that of the [HgS₄] tetrahedron (Table S6), which implies that the [GeOS₃] unit has a significant contribution to the large birefringence of Sr₂HgGe₂OS₆.

CONCLUSIONS

In summary, the first Hg-based oxychalcogenide IR NLO material $Sr_2HgGe_2OS_6$ with mixed-anion $[GeOS_3]$ units was successfully synthesized through the spontaneous crystallization method, which crystallizes in the NCS tetragonal space group $P\overline{4}2_1m$. The crystal structure of $Sr_2HgGe_2OS_6$ consists of 2D $[HgGe_2OS_6]_{\infty}$ layers stacking separated by Sr^{2+} cations to balance the charge. It exhibits well-balanced NLO performance, featuring the strong SHG response $(0.7 \times AGS)$, large experimental band gap (2.9 eV), high LIDT $(2.1 \times AGS)$ as well as large birefringence (0.128@2090 nm), and appropriate PM behavior. Our research indicates that due to the unique properties of Hg atoms, such as large polarizability and large radius, the introduction of Hg atoms is also very advantageous for improving the NLO performance of oxychalcogenides.

ASSOCIATED CONTENT

Supporting Information

The Supporting Information is available free of charge at https://pubs.acs.org/doi/10.1021/acs.inorgchem.4c00959.

Wyckoff site, fractional atomic coordinates, equivalent isotropic displacement parameters $U_{\rm eq}$ and BVS, selected

bond lengths and bond angles, powder LIDTs, DM direction and magnitude, and element content and distribution (PDF)

Accession Codes

CCDC 2324769 contains the supplementary crystallographic data for this paper. These data can be obtained free of charge via www.ccdc.cam.ac.uk/data_request/cif, or by emailing data_request@ccdc.cam.ac.uk, or by contacting The Cambridge Crystallographic Data Centre, 12 Union Road, Cambridge CB2 1EZ, UK; fax: +44 1223 336033.

AUTHOR INFORMATION

Corresponding Authors

Ming-Hsien Lee – Department of Physics, Tamkang University, New Taipei 25137, Taiwan; orcid.org/0000-0003-3956-181X; Email: mhslee@mail.tku.edu.tw

Jiyong Yao — Beijing Center for Crystal Research and Development, Key Lab of Functional Crystals and Laser Technology, Technical Institute of Physics and Chemistry, Chinese Academy of Sciences, Beijing 100190, P. R. China; Center of Materials Science and Optoelectronics Engineering, University of Chinese Academy of Sciences, Beijing 100049, P. R. China; orcid.org/0000-0002-4802-5093; Email: jyao@mail.ipc.ac.cn

Authors

Guili Wang — Beijing Center for Crystal Research and Development, Key Lab of Functional Crystals and Laser Technology, Technical Institute of Physics and Chemistry, Chinese Academy of Sciences, Beijing 100190, P. R. China; Center of Materials Science and Optoelectronics Engineering, University of Chinese Academy of Sciences, Beijing 100049, P. R. China; University of Chinese Academy of Sciences, Beijing 100049, P. R. China

Chunxiao Li — Beijing Center for Crystal Research and Development, Key Lab of Functional Crystals and Laser Technology, Technical Institute of Physics and Chemistry, Chinese Academy of Sciences, Beijing 100190, P. R. China

Complete contact information is available at: https://pubs.acs.org/10.1021/acs.inorgchem.4c00959

Author Contributions

Guili Wang: methodology, characterization, data curation, validation, writing—original draft, and writing—review and editing. Chunxiao Li: supervised the powder SHG measurement. Ming-Hsien Lee: theoretical calculations. Jiyong Yao: funding acquisition, resources, data curation, and writing—review and editing.

Notes

The authors declare no competing financial interest.

ACKNOWLEDGMENTS

This work was supported by the National Natural Science Foundation of China (no. 22175190).

REFERENCES

- (1) Das, S.; Ghosh, C.; Gangopadhyay, S. A comparative study of second harmonic generation of pulsed CO₂ laser radiation in some infrared crystals. *Infrared Phys. Technol.* **2007**, *51*, 9–12.
- (2) Harimoto, T. Evaluation of Stable Optical Parametric Amplification Involving Temporal Distribution. *Jpn. J. Appl. Phys.* **2003**, *42*, 3415–3418.

- (3) Mangin, J.; Mennerat, G.; Gadret, G.; Badikov, V.; de Miscault, J.-C. Comprehensive formulation of temperature-dependent dispersion of optical materials: illustration with case of temperature tuning of a mid-IR HgGa₂S₄ OPO. *J. Opt. Soc. Am. B* **2009**, *26*, 1702–1709.
- (4) Luo, X.; Li, Z.; Guo, Y.; Yao, J.; Wu, Y. Recent progress on new infrared nonlinear optical materials with application prospect. *J. Solid State Chem.* **2019**, *270*, *674*–*687*.
- (5) Gong, P.; Liang, F.; Kang, L.; Chen, X.; Qin, J.; Wu, Y.; Lin, Z. Recent advances and future perspectives on infrared nonlinear optical metal halides. *Coord. Chem. Rev.* **2019**, *380*, 83–102.
- (6) Pestov, D.; Wang, X.; Ariunbold, G. O.; Murawski, R. K.; Sautenkov, V. A.; Dogariu, A.; Sokolov, A. V.; Scully, M. O. Singleshot detection of bacterial endospores via coherent Raman spectroscopy. *Proc. Natl. Acad. Sci. U.S.A.* **2008**, *105*, 422–427.
- (7) Serebryakov, V. A.; Boĭko, É. V.; Petrishchev, N. N.; Yan, A. V. Medical applications of mid-IR lasers. Problems and prospects. *J. Opt. Technol.* **2010**, *77*, 6–17.
- (8) Abudurusuli, A.; Li, J.; Pan, S. A review on the recently developed promising infrared nonlinear optical materials. *Dalton Trans.* **2021**, *50*, 3155–3160.
- (9) Boyd, G. D.; Buehler, E.; Storz, F. G. Linear and nonlinear optical properties of ZnGeP₂ and CdSe. *Appl. Phys. Lett.* **1971**, *18*, 301–304.
- (10) Chemla, D. S.; Kupecek, P. J.; Robertson, D. S.; Smith, R. C. Silver thiogallate, a new material with potential for infrared devices. *Opt. Commun.* **1971**, *3*, 29–31.
- (11) Boyd, G.; Kasper, H.; McFee, J.; Storz, F. Linear and nonlinear optical properties of some ternary selenides. *IEEE J. Quantum Electron.* **1972**, *8*, 900–908.
- (12) Akiko Harasaki, A. H.; Kiyoshi Kato, K. K. New Data on the Nonlinear Optical Constant, Phase-Matching, and Optical Damage of AgGaS₂. *Jpn. J. Appl. Phys.* **1997**, *36*, 700.
- (13) Catella, G. C.; Shiozawa, L. R.; Hietanen, J. R.; Eckardt, R. C.; Route, R. K.; Feigelson, R. S.; Cooper, D. G.; Marquardt, C. L. Mid-IR absorption in AgGaSe₂ optical parametric oscillator crystals. *Appl. Opt.* **1993**, 32, 3948–3951.
- (14) Zhong, K.; Liu, C.; Wang, M.; Shi, J.; Kang, B.; Yuan, Z.; Li, J.; Xu, D.; Shi, W.; Yao, J. Linear optical properties of ZnGeP₂ in the terahertz range. *Opt. Mater. Express* **2017**, *7*, 3571–3579.
- (15) Guo, S.-P.; Chi, Y.; Guo, G.-C. Recent achievements on middle and far-infrared second-order nonlinear optical materials. *Coord. Chem. Rev.* **2017**, 335, 44–57.
- (16) Wang, S.; Zhan, M.; Wang, G.; Xuan, H.; Zhang, W.; Liu, C.; Xu, C.; Liu, Y.; Wei, Z.; Chen, X. 4H-SiC: a new nonlinear material for midinfrared lasers. *Laser Photonics Rev.* **2013**, *7*, 831–838.
- (17) Zhou, W.; Guo, S.-P. Rational Design of Novel Promising Infrared Nonlinear Optical Materials: Structural Chemistry and Balanced Performances. *Acc. Chem. Res.* **2024**, *57*, 648–660.
- (18) Yan, H.; Matsushita, Y.; Yamaura, K.; Tsujimoto, Y. La₃Ga₃Ge₂S₃O₁₀: An Ultraviolet Nonlinear Optical Oxysulfide Designed by Anion-Directed Band Gap Engineering. *Angew. Chem., Int. Ed.* **2021**, *60*, 26561–26565.
- (19) Wang, R.; Guo, Y.; Zhang, X.; Xiao, Y.; Yao, J.; Huang, F. Sr₅Ga₈O₃S₁₄: A Nonlinear Optical Oxysulfide with Melilite-Derived Structure and Wide Band Gap. *Inorg. Chem.* **2020**, *59*, 9944–9950.
- (20) Cui, S.; Wu, H.; Hu, Z.; Wang, J.; Wu, Y.; Yu, H. The Antiperovskite-Type Oxychalcogenides Ae₃Q[GeOQ₃] (Ae = Ba, Sr; Q = S, Se) with Large Second Harmonic Generation Responses and Wide Band Gaps. *Adv. Sci.* 2023, 10, 2204755.
- (21) Zhang, \hat{X} .; Xiao, Y.; Wang, R.; Fu, P.; Zheng, C.; Huang, F. Synthesis, crystal structures and optical properties of noncentrosymmetric oxysulfides AeGeS₂O (Ae = Sr, Ba). *Dalton Trans.* **2019**, 48, 14662–14668.
- (22) Wang, R.; Liang, F.; Liu, X.; Xiao, Y.; Liu, Q.; Zhang, X.; Wu, L.-M.; Chen, L.; Huang, F. Heteroanionic Melilite Oxysulfide: A Promising Infrared Nonlinear Optical Candidate with a Strong Second-Harmonic Generation Response, Sufficient Birefringence, and Wide Bandgap. ACS Appl. Mater. Interfaces 2022, 14, 23645–23652.

- (23) Endo, T.; Doi, Y.; Wakeshima, M.; Suzuki, K.; Matsuo, Y.; Tezuka, K.; Ohtsuki, T.; Shan, Y. J.; Hinatsu, Y. Magnetic Properties of the Melilite-Type Oxysulfide Sr₂MnGe₂S₆O: Magnetic Interactions Enhanced by Anion Substitution. *Inorg. Chem.* **2017**, *56*, 2459–2466.
- (24) Ran, M.-Y.; Zhou, S.-H.; Li, B.; Wei, W.; Wu, X.-T.; Lin, H.; Zhu, Q.-L. Enhanced Second-Harmonic-Generation Efficiency and Birefringence in Melillite Oxychalcogenides Sr₂MGe₂OS₆ (M = Mn, Zn, and Cd). *Chem. Mater.* **2022**, *34*, 3853–3861.
- (25) Yang, H.-D.; Zhou, S.-H.; Ran, M.-Y.; Wu, X.-T.; Lin, H.; Zhu, Q.-L. Melilite oxychalcogenide Sr₂FeGe₂OS₆: a phase-matching IR nonlinear optical material realized by isomorphous substitution. *Inorg. Chem. Front.* **2023**, *10*, 2030–2038.
- (26) Zhang, N.; Xu, Q.-T.; Shi, Z.-H.; Yang, M.; Guo, S.-P. Characterizations and Nonlinear-Optical Properties of Pentanary Transition-Metal Oxysulfide Sr₂CoGe₂OS₆. *Inorg. Chem.* **2022**, *61*, 17002–17006.
- (27) Tian, X.; Zhang, X.; Xiao, Y.; Wu, X.; Zhang, B.; Yang, D.; Wu, K. From oxides to oxysulfides: the mixed-anion GeS_3O unit induces huge improvement in the nonlinear optical effect and optical anisotropy for potential nonlinear optical materials. *RSC Adv.* **2022**, 12, 16296–16300.
- (28) Cheng, Y.; Wu, H.; Yu, H.; Hu, Z.; Wang, J.; Wu, Y. Rational design of a promising oxychalcogenide infrared nonlinear optical crystal. *Chem. Sci.* **2022**, *13*, 5305–5310.
- (29) Zhang, N.; Huang, X.; Yao, W.-D.; Chen, Y.; Pan, Z.-R.; Li, B.; Liu, W.; Guo, S.-P. Eu₂MGe₂OS₆ (M = Mn, Fe, Co): Three Melilite-Type Rare-Earth Oxythiogermanates Exhibiting Balanced Nonlinear-Optical Behaviors. *Inorg. Chem.* **2023**, *62*, 16299–16303.
- (30) Xing, W.; Fang, P.; Wang, N.; Li, Z.; Lin, Z.; Yao, J.; Yin, W.; Kang, B. Two Mixed-Anion Units of [GeOSe₃] and [GeO₃S] Originating from Partial Isovalent Anion Substitution and Inducing Moderate Second Harmonic Generation Response and Large Birefringence. *Inorg. Chem.* **2020**, *59*, 16716–16724.
- (31) Sun, M.; Xing, W.; Lee, M.-H.; Yao, J. Bridging oxygen atoms in trigonal prism units driven strong second-harmonic-generation efficiency in Sr₃Ge₂O₄Te₃. *Chem. Commun.* **2022**, *58*, 11167–11170.
- (32) Sun, M.; Zhang, X.; Li, C.; Liu, W.; Lin, Z.; Yao, J. Highly polarized [GeOTe₃] motif-driven structural order promotion and an enhanced second harmonic generation response in the new nonlinear optical oxytelluride Ba₃Ge₂O₄Te₃. *J. Mater. Chem. C* **2022**, *10*, 150–159.
- (33) Li, J.-N.; Li, X.-H.; Xu, Y.-X.; Liu, W.; Guo, S.-P. First Investigation of Nonlinear Optical Oxychalcogenide with Three-Dimensional Anionic Framework and Special Windmill-Like Functional Motifs. *Chin. J. Chem.* **2022**, *40*, 2407–2414.
- (34) Yang, M.; Yao, W.-D.; Liu, W.; Guo, S.-P. The first quaternary rare-earth oxythiogermanate with second-harmonic generation and ferromagnetic behavior. *Chem. Commun.* **2023**, *59*, 3894–3897.
- (35) Ran, M.-Y.; Ma, Z.; Chen, H.; Li, B.; Wu, X.-T.; Lin, H.; Zhu, Q.-L. Partial Isovalent Anion Substitution to Access Remarkable Second-Harmonic Generation Response: A Generic and Effective Strategy for Design of Infrared Nonlinear Optical Materials. *Chem. Mater.* **2020**, 32, 5890–5896.
- (36) Li, C.; Meng, X.; Li, Z.; Yao, J. Hg-based chalcogenides: An intriguing class of infrared nonlinear optical materials. *Coord. Chem. Rev.* **2022**, 453, 214328.
- (37) Zhang, Y.; Wu, H.; Hu, Z.; Wang, J.; Wu, Y.; Yu, H. Achieving a strong second harmonic generation response and a wide band gap in a Hg-based material. *Inorg. Chem. Front.* **2022**, *9*, 4075–4080.
- (38) Yan, M.; Sun, Z.-D.; Yao, W.-D.; Zhou, W.; Liu, W.; Guo, S.-P. A highly distorted HgS₄ tetrahedron-induced moderate second-harmonic generation response of EuHgGeS₄. *Inorg. Chem. Front.* **2020**, *7*, 2451–2458.
- (39) Wu, K.; Su, X.; Pan, S.; Yang, Z. Synthesis and Characterization of Mid-Infrared Transparency Compounds: Acentric BaHgS₂ and Centric Ba₈Hg₄S₅Se₇. *Inorg. Chem.* **2015**, *54*, 2772–2779.
- (40) Li, C.; Yin, W.; Gong, P.; Li, X.; Zhou, M.; Mar, A.; Lin, Z.; Yao, J.; Wu, Y.; Chen, C. Trigonal Planar [HgSe₃]⁴⁻ Unit: A New Kind of Basic Functional Group in IR Nonlinear Optical Materials

- with Large Susceptibility and Physicochemical Stability. J. Am. Chem. Soc. 2016, 138, 6135–6138.
- (41) Bourhis, L. J.; Dolomanov, O. V.; Gildea, R. J.; Howard, J. A. K.; Puschmann, H. The anatomy of a comprehensive constrained, restrained refinement program for the modern computing environment Olex2 dissected. *Acta Crystallogr., Sect. A: Found. Adv.* 2015, 71, 59–75.
- (42) Sheldrick, G. M. Crystal structure refinement with SHELXL. *Acta Crystallogr., Sect. C: Struct. Chem.* **2015**, *71*, 3–8.
- (43) Simmons, E. L. Diffuse reflectance spectroscopy: a comparison of the theories. *Appl. Opt.* **1975**, *14*, 1380–1386.
- (44) Kurtz, S. K.; Perry, T. T. A Powder Technique for the Evaluation of Nonlinear Optical Materials. *J. Appl. Phys.* **1968**, 39, 3798–3813.
- (45) Zhang, M.-J.; Jiang, X.-M.; Zhou, L.-J.; Guo, G.-C. Two phases of Ga₂S₃: promising infrared second-order nonlinear optical materials with very high laser induced damage thresholds. *J. Mater. Chem. C* **2013**, *1*, 4754–4760.
- (46) Segall, M. D.; Lindan, P. J. D.; Probert, M. J.; Pickard, C. J.; Hasnip, P. J.; Clark, S. J.; Payne, M. C. First-principles simulation: ideas, illustrations and the CASTEP code. *J. Phys.: Condens. Matter* **2002**, *14*, 2717–2744.
- (47) Perdew, J. P.; Burke, K.; Ernzerhof, M. Generalized Gradient Approximation Made Simple. *Phys. Rev. Lett.* **1996**, 77, 3865–3868.
- (48) Hamann, D. R.; Schlüter, M.; Chiang, C. Norm-Conserving Pseudopotentials. *Phys. Rev. Lett.* **1979**, 43, 1494–1497.
- (49) Yao, W.-D.; Huang, X.; Yan, M.; Liu, W.; Guo, S.-P. $KHg_4Ga_3S_9$: A Hg-Based Sulfide with Nonlinear-Optical Activity in the A- M^{II} - M^{III} -Q (A = Alkali Metal; M^{II} = G^{II} Metal; M^{III} = G^{II} Ga, In; Q^{II} = G^{II} System. *Inorg. Chem.* **2023**, *62*, 12639–12643.
- (50) Golovnev, N. N.; Molokeev, M. S.; Vereshchagin, S. N.; Atuchin, V. V.; Sidorenko, M. Y.; Dmitrushkov, M. S. Crystal structure and properties of the precursor $[Ni(H_2O)_6](HTBA)_2 \cdot 2H_2O$ and the complexes $M(HTBA)_2(H_2O)_2$ (M = Ni, Co, Fe). *Polyhedron* **2014**, 70, 71–76.
- (51) Denisenko, Y. G.; Molokeev, M. S.; Oreshonkov, A. S.; Krylov, A. S.; Aleksandrovsky, A. S.; Azarapin, N. O.; Andreev, O. V.; Razumkova, I. A.; Atuchin, V. V. Crystal Structure, Vibrational, Spectroscopic and Thermochemical Properties of Double Sulfate Crystalline Hydrate [CsEu(H₂O)₃(SO₄)₂]·H₂O and Its Thermal Dehydration Product CsEu(SO₄)₂. Crystals **2021**, *11*, 1027.
- (52) Lin, H.; Chen, L.; Zhou, L.-J.; Wu, L.-M. Functionalization based on the substitutional flexibility: strong middle IR nonlinear optical selenides $AX_{4}^{II}X_{5}^{III}Se_{12}$. J. Am. Chem. Soc. **2013**, 135, 12914–12921.
- (53) Babu, G. A.; Raja, R. S.; Ramasamy, P.; Karunagaran, N. Growth improvement and characterization of AgGaSe₂ chalcopyrite single crystals using Bridgman technique. *AIP Conf. Proc.* **2012**, *1447*, 1045–1046.
- (54) Zhao, X.; Zhu, S.; Zhao, B.; Chen, B.; He, Z.; Wang, R.; Yang, H.; Sun, Y.; Cheng, J. Growth and characterization of ZnGeP₂ single crystals by the modified Bridgman method. *J. Cryst. Growth* **2008**, 311, 190–193.
- (55) Li, M.-Y.; Li, B.; Lin, H.; Ma, Z.; Wu, L.-M.; Wu, X.-T.; Zhu, Q.-L. Sn₂Ga₂S₅: A Polar Semiconductor with Exceptional Infrared Nonlinear Optical Properties Originating from the Combined Effect of Mixed Asymmetric Building Motifs. *Chem. Mater.* **2019**, *31*, 6268–6275.
- (56) Kleinman, D. A. Nonlinear Dielectric Polarization in Optical Media. *Phys. Rev.* **1962**, *126*, 1977–1979.
- (57) Maggard, P. A.; Nault, T. S.; Stern, C. L.; Poeppelmeier, K. R. Alignment of acentric $MoO_3F_3^{3-}$ anions in a polar material: $(Ag_3MoO_3F_3)(Ag_3MoO_4)$ Cl. J. Solid State Chem. **2003**, 175, 27–33.